BBA - General Subjects 1862 (2018) 1843–1851

Contents lists available at ScienceDirect

BBA - General Subjects

journal homepage: www.elsevier.com/locate/bbagen

Structural insights into operator recognition by BioQ in the *Mycobacterium smegmatis* biotin synthesis pathway

Ling Yan[a,1], Qing Tang[a,b,1], Zeyuan Guan[a,c], Kai Pei[a], Tingting Zou[a,*], Jin He[a,b,*]

[a] College of Life Science and Technology, Huazhong Agricultural University, Wuhan, Hubei 430070, China
[b] State Key Laboratory of Agricultural Microbiology, Huazhong Agricultural University, Wuhan, Hubei 430070, China
[c] National Key Laboratory of Crop Genetic Improvement and National Centre of Plant Gene Research, Huazhong Agricultural University, Wuhan, Hubei 430070, China

ARTICLE INFO

Keywords:
Biotin
TetR family
BioQ
Mycobacterium
Crystal structure
Translation regulation
Protein–DNA interaction

ABSTRACT

Background: Biotin is an essential cofactor in living organisms. The TetR family transcriptional regulator (TFTR) BioQ is the main regulator of biotin synthesis in *Mycobacterium smegmatis*. BioQ represses the expression of its target genes by binding to a conserved palindromic DNA sequence (the BioQ operator). However, the mechanism by which BioQ recognizes this DNA element has not yet been fully elucidated.

Methods/results: We solved the crystal structures of the BioQ homodimer in its apo-form and in complex with its specific operator at 2.26 Å and 2.69 Å resolution, respectively. BioQ inserts the N-terminal recognition helix of each protomer into the corresponding major grooves of its operator and stabilizes the formation of the complex via electrostatic interactions and hydrogen bonding to induce conformational changes in both the DNA and BioQ. The DNA interface of BioQ is rich in positively charged residues, which help BioQ stabilize DNA binding. We elucidated the structural basis of DNA recognition by BioQ for the first time and identified the amino acid residues responsible for DNA binding via further site-directed mutagenesis.

General significance: Our findings clearly elucidate the mechanism by which BioQ recognizes its operator in the biotin synthesis pathway and reveal the unique structural characteristics of BioQ that are distinct from other TFTR members.

1. Introduction

Biotin (vitamin H) is an essential cofactor for a class of metabolic enzymes that catalyze crucial carboxylation, decarboxylation and transcarboxylation reactions in every domain of life [1–3]. Biotin starvation or deficiencies potentially lead to mortality [1,4]. While bacteria, most fungi and plants synthesize biotin de novo, mammals lack biotin synthesis-related enzymes and need to obtain biotin from exogenous food or the gastrointestinal microbiota [5–7]. Although bacteria harness various pathways to synthesize the biotin precursor pimeloyl-CoA [2,3], the enzymes that synthesize biotin from pimeloyl-CoA are encoded by universal genes, including *bioF*, *bioA*, *bioD* and *bioB*, in a wide variety of bacteria [8–10]. These genes are always present in clusters and are strictly controlled by the three different types of biotin regulatory systems that respond to intracellular biotin levels [2]. Therefore, inhibition of the biotin synthetic pathway or biotin uptake process may represent a novel anti-bacterial strategy [11,12].

The biotin regulatory system in the γ-*Proteobacteria* and *Bacillus/Clostridium* groups depends on the bifunctional BirA protein, which acts both as a biotin-protein ligase (BPL) that mediate the biotinylation of biotin-dependent carboxylase, and as a transcriptional repressor of biotin synthesis genes (*bio* operons) [2,8,13]. However, BirA proteins from α-*Proteobacteria* and *Actinobacteria* lack the N-terminal DNA-binding domain (DBD) and require other transcription regulators to compensate for the loss of regulatory function [13]. The GntR-type transcriptional regulator BioR is reported to take over the transcriptional regulatory role of BirA in most α-*Proteobacteria*, constituting the biotin regulatory system along with BirA [5,8]. In *Actinobacteria*, a conserved protein, BioQ—a TetR family transcriptional regulator (TFTR) —recognizes the *bio* operons via a 13-bp palindromic inverted repeat sequence (5′-TGAACnnnGTTCA-3′) and regulates gene expression as a transcriptional repressor [14,15] (Fig. 1A). Although the organization of the *bio* operons is not completely identical throughout the phylum *Actinobacteria*, BioQ and its recognition sites in the promoter region (the BioQ-operator) of *bio* operons are highly conserved [14,15]. To date, the mechanism by which BioQ regulates biotin synthesis is unknown.

Previously, we described the BioQ-regulatory system in

* Corresponding authors.
E-mail addresses: zoutingting@mail.hzau.edu.cn (T. Zou), hejin@mail.hzau.edu.cn (J. He).
[1] Both authors contributed equally to this work.

https://doi.org/10.1016/j.bbagen.2018.05.015
Received 10 November 2017; Received in revised form 18 April 2018; Accepted 19 May 2018
Available online 28 May 2018

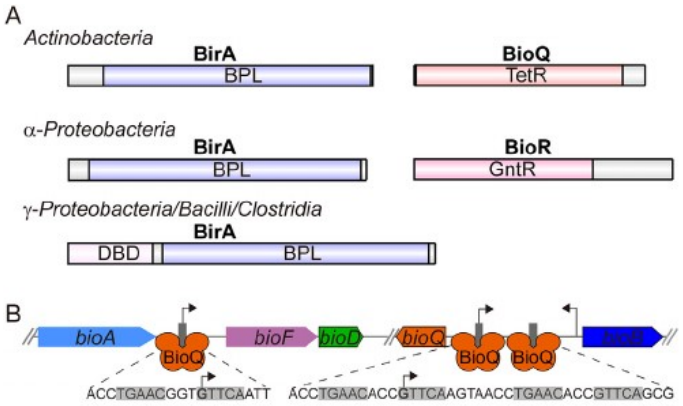

Fig. 1. Schemes of gene transcriptional repression by BioQ. (A) Biotin regulatory systems in different bacteria. BirA of γ-*Proteobacteria*, *Bacilli* and *Clostridia* is a bifunctional protein that contains both a BPL and a DBD. However, *Actinobacteria* and α-*Proteobacteria* both lack a DBD and depend on the transcriptional regulator BioQ or BioR to compensate for its role in gene regulation. (B) Crucial genes for biotin synthesis are repressed by BioQ. BioQ binds to the promoter region of the *bioF-D* operon and to the *bioQ* and *bioB* genes by recognizing a conserved palindromic sequence (5′-TGAACnnnGTTCA-3′) in the genome of *M. smegmatis*. Conserved palindromic sequences are shaded. The bent arrows indicate the transcriptional start sites (TSSs).

Mycobacterium smegmatis. As a transcriptional repressor, BioQ binds to three operators located in the promoter regions of the *bioB* and *bioF/D* operons and its own coding gene, *bioQ*. The antisense promoter of *bioQ* and the sense promoter of *bioB* partially overlap and contain two tandem BioQ operator sites, which overlap with or are downstream of the transcriptional start sites (TSSs) [14] (Fig. 1B). However, the molecular mechanisms by which BioQ recognizes its target genes remains to be elucidated.

TFTR members play important regulatory roles in controlling the pathogenicity, metabolism, cell stress, and multidrug and metal resistance in bacteria in response to numerous environmental changes [16–20]. TFTR members possess an N-terminal helix-turn-helix (HTH) DBD and a C-terminal ligand-binding domain (LBD) [18,19,21]. Typically, the TFTR recognizes the operator sites as a homodimer. Upon ligand binding, the LBD of canonical TFTRs undergoes a subtle conformational change to allosterically trigger the DBD to disrupt its DNA-binding activity [21]. Noncanonical TFTRs possess different ligand regulatory mechanisms; some TFTRs bind with more than one ligand, and their DNA-binding ability changes upon binding to different ligands [22–24]. Compared with the highly conserved DBDs, the sequences and structures of LBDs are more variable to sense diverse types of ligands [19].

In the current study, we solved the crystal structure of *M. smegmatis* BioQ with and without the operator DNA at 2.26 Å and 2.69 Å resolution, respectively. BioQ exhibits typical TFTR folding but lacks a short helix in the LBD. BioQ binds to its cognate operator through the DBDs of each monomer and induces the conformational changes in the DNA operator. In addition to performing biochemical studies, we determined the critical amino acid residues responsible for the BioQ-operator interaction. Our study not only offers molecular insights into the biotin synthesis pathway controlled by BioQ, which is widely utilized by *Mycobacterium*, but also provides a framework for ligand identification.

2. Materials and methods

2.1. Bacterial strains and growth conditions

M. smegmatis MC^2 155 was grown at 37 °C in Middlebrook 7H9 broth (BD, USA) supplemented with 0.2% glycerol and 0.05% Tween 80. *Escherichia coli* DH5α and *E. coli* BL21(DE3) were grown in lysogeny broth (LB) at 37 °C. When necessary, appropriate antibiotics were added to the cultures at the following final concentrations: kanamycin, 25 μg/ml for *M. smegmatis* and 50 μg/ml for *E. coli*.

2.2. Cloning, expression and purification

Full-length and truncated *bioQ* genes were amplified from the genomic DNA of *M. smegmatis* MC^2 155. Nested PCR was carried out for the site-directed mutagenesis of *bioQ* using designed primers (Table S1). The corresponding genes were cloned into pET15 (Novagen, USA) to generate C-terminal hexa-histidine-tagged fusion proteins. All clones were verified by DNA sequencing.

The sequenced recombinant vectors were transformed into *E. coli* BL21(DE3) and grown in LB broth supplemented with 100 μg/ml ampicillin at 37 °C until the cell density reached an OD of 1.0–1.2 at A600. Protein expression was induced by adding 0.2 mM isopropyl-β-D-thiogalactoside (IPTG), and cells were grown at 16 °C for 12 h. Then, the cells were spun down at 4 °C and resuspended in buffer A (25 mM Tris-HCl, pH 8.0, 150 mM NaCl). The cells were lysed using a high-pressure cell disrupter (JNBIO, China), and cell debris was removed by centrifugation at 20,000 × *g* for 1 h at 4 °C. The supernatant was loaded onto a Ni-NTA resin column (Qiagen, Germany), washed with buffer B (25 mM Tris-HCl, pH 8.0, 150 mM NaCl, 15 mM imidazole), and eluted with buffer C (25 mM Tris-HCl, pH 8.0, 250 mM imidazole) to acquire the hexa-histidine-tagged fusion protein. The protein was further purified via anion exchange chromatography (Source 15Q, GE Healthcare, USA) using a linear NaCl gradient in buffer A. Then, the hexa-histidine-tag was removed by digesting the sample with drICE protease for 1 h on ice and separating the sample using gel filtration chromatography (Superdex-200 Increase10/300 GL, GE Healthcare) in a lysis buffer containing 25 mM Tris-HCl, pH 8.0, 150 mM NaCl and 5 mM dithiothreitol. Selenomethionine (Se-Met)-labeled protein was expressed in a Se-Met-containing medium (ACROS, USA). The purity of the protein was analyzed by sodium dodecyl sulfate polyacrylamide gel electrophoresis (SDS-PAGE), and the purified fractions from the gel filtration chromatography were collected for crystallization. The protein was quantified using a NanoDrop 2000 spectrophotometer (Thermo Scientific, USA) at an extinction coefficient of 20,970 and stored at −80 °C after flash freezing in liquid nitrogen.

2.3. Crystallization

Crystallization screening of apo-BioQ was performed using the sitting-drop vapor-diffusion method at 18 °C by mixing an equal volume (1 μl) of 10 mg/ml protein with various reservoir solutions. A full-length BioQ (residues 1–205) crystal appeared in the reservoir solution containing 0.2 M ammonium sulfate, 100 mM Bis-Tris pH 6.5, and 22% (*w/v*) polyethylene glycol 3350. However, the diffraction was poor. A series of BioQ truncations were further constructed to improve the diffraction of crystals. Crystals of BioQ (residues 1–188) that diffracted well were finally obtained in the well containing 22% (w/v) polyethylene glycol 3350, 100 mM Bis-Tris pH 6.1, 0.2 M ammonium sulfate, and 4% (*v/v*) polypropylene glycol P 400 via the hanging-drop vapor-diffusion method at 18 °C. In addition, 13.3% (v/v) glycerol was included in the reservoir solution as a cryoprotective buffer. The apo-BioQ crystals were found to diffract beyond 2.26 Å at the Shanghai Synchrotron Radiation Facility (SSRF) on beamline BL17U.

To crystalize the BioQ-operator complex, 13-, 15-, 17-, 19-, 21-, 23-, 25- and 27-bp double-stranded DNA (dsDNA) molecules containing the 13-bp palindromic inverted repeat sequence (5′-TGAACACCGTTCA-3′) were incubated with BioQ (residues 1–188), and their binding affinities were measured via isothermal titration calorimetry (ITC) (Fig. S1). The binding affinity of BioQ with the 19-bp probe (5′-ACCTGAACACCGTTCAAGT-3′) was notably stronger than that with the 13- and 15-bp probes, but similar to that of the other DNA probes. Therefore, the 19-bp dsDNA (19-mer) probe was synthesized, purified by HPLC, and used for crystallization. To obtain crystals of the BioQ-operator complex,

Table 1
Statistics of data collection and refinement.

Processing Structure	BioQ-Apo	BioQ-DNA	BioQ-DNA (Se-Met)
Wavelength (Å)	0.9778	0.9792	0.9793
Resolution range (Å)[a]	45–2.26 (2.26–2.19)	45–2.69 (2.82–2.69)	45–2.90 (3.08–2.90)
Space group	I 1 2 1	C 2	C 2
Unit cell parameters (Å, °)	a = 37.9	a = 60.8	a = 58.4
	b = 193.9	b = 213.1	b = 214.5
	c = 54.0	c = 88.9	c = 93.3
	90	90	90
	100.2	99.56	96.3
	90	90	90
Unique reflections	19,546	29,957	25,086
Multiplicity	6.6 (6.3)	7.3 (7.1)	10.6 (10.7)
Completeness (%)	99.3 (93.4)	98 (90.2)	99.6 (99.3)
$< I > / < \sigma I >$	9.5 (2.2)	7.7 (1.8)	12.0 (0.8)
CC(1/2)[c]	0.99 (0.77)	0.99 (0.86)	0.99 (0.40)
Wilson B factor ($Å^2$)	39.1	64.1	103.2
R_{merge}[b](%)	11.4 (65.5)	11.0 (92.3)	17.2 (392.6)
Refinement			
Resolution range (Å)	45–2.26	45–2.69	
R_{work} /R_{free}[d](%)	21.2/24.7	21.3/26.7	
Average B factor ($Å^2$) (No of atoms)			
protein	53.29 (2582)	102.4 (3837)	
DNA		106.9 (1155)	
solvent	52.91 (74)	92.6 (4)	
Rmsd bond lengths (Å)	0.015	0.008	
Rmsd bond angles (°)	1.238	1.033	
Ramachandran favored[e] (%)	96.3	90.7	
Ramachandran Additionally allowed (%)	3.7	9.3	
Ramachandran outliers (%)	0	0	

[a] Values in parentheses correspond to the highest resolution shell.
[b] $R_{merge} = \Sigma_h\Sigma_i|I_{h,i}-I_h|/\Sigma_h\Sigma_i I_{h,i}$, where I_h is the mean intensity of the i observations of symmetry-related reflections of h.
[c] As defined by Karplus [65].
[d] $R = \Sigma h|Fo-Fc|/\Sigma h|Fo|$ for all reflections, where Fo and Fc are the observed and calculated structure factors, respectively. R_{free} is calculated analogously for the test reflections, randomly selected and excluded from the refinement.
[e] As defined using Molprobity [66].

10 mg/ml of purified BioQ or Se-Met-labeled BioQ was mixed with reannealed 19-mer DNA at a molar ratio of 1:1.5 (BioQ:DNA) and incubated on ice for 30 min before crystallization. Co-crystallization trials of BioQ-DNA were performed using the hanging-drop vapor-diffusion method at 18 °C by mixing 1 μl of the sample with an equal volume of reservoir solution. Needle-shaped crystals appeared overnight in the reservoir solution containing 12% (*w/v*) polypropylene glycol 8000, 100 mM MOPS and HEPES, pH 7.5, 0.15 M magnesium acetate, and 3% (*v*/v) 1-propanol. After 36 h of growth, the crystal matured and was flash-frozen in liquid nitrogen, and 17% (v/v) glycerol was added to the reservoir solution as a cryoprotective buffer. The crystals of the BioQ-DNA complex diffracted beyond 2.69 Å at the SSRF on beamline BL17U.

2.4. Data collection and structure determination

All data sets were collected at the SSRF on beamline BL17U [25] and processed with the HKL2000 program and XDS packages [26]. Further data processing was carried out using the CCP4 program suite [27]. The structure of the BioQ-DNA complex was solved according to the single wavelength anomalous diffraction (SAD) method. Data collection and structure refinement statistics are summarized in Table 1. The structure of apo-BioQ was solved by molecular replacement using the BioQ-DNA complex as the search model with the PHASER program [28]. The structures were built using COOT and iteratively refined using the PHENIX program [29,30]. All figures were generated using the PyMOL program (http://www.pymol.org/).

2.5. Construction of the ΔbioQ complementary strain

The *bioQ* (*MSMEG_3193*) deletion mutant of *M. smegmatis* MC^2 155 was constructed in a previous study [14]. The *bioQ* gene and its site mutants were cloned into the pMV261 vector and transformed into Δ*bioQ* by electroporation.

2.6. Quantitative reverse transcription PCR (qRT-PCR)

M. smegmatis grown in Middlebrook 7H9 broth supplemented with 25 μg/ml kanamycin was grown to the mid-logarithmic growth phase and collected to isolate total RNA using TRIzol reagent (Life Technologies, USA). cDNAs were synthesized using the PrimeScript RT Kit with gDNA Eraser (Takara Biotechnology, Japan) according to the manufacturer's instructions. qRT-PCR was performed as described previously [14] using cDNAs as the template with the primers listed in Table S1. The 16S rRNA gene was used-as the internal reference, and the relative gene expression changes were calculated using the $2^{-\Delta\Delta Ct}$ method.

2.7. Electrophoretic mobility shift assays (EMSAs)

First, 5′-FAM fluorescence-labeled DNA probes were synthesized (Tianyi Biotech, China), and 100 nM probes were incubated with various amounts of the BioQ protein in an EMSA buffer (25 mM Tris-HCl, pH 8.0, 10 mM $MgCl_2$, 150 mM NaCl, 50 ng/ml heparin and 10% glycerol) at 4 °C for 30 min. Then, the reaction mixtures were subjected to

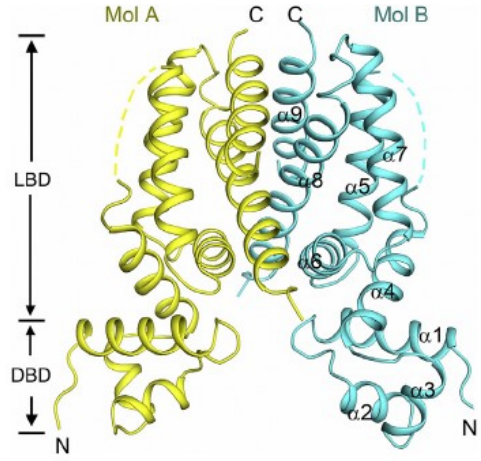

Fig. 2. Overall structure of the BioQ homodimer. The two subunits of the homodimer are colored in cyan and yellow, respectively. The N- and C– termini, the LBD and DBD are indicated. In one monomer, the helices are labeled sequentially as α1 to α9.

6% native-PAGE in 0.5× Tris-glycine buffer under an electric field of 15 V/cm for 2.5 h. Images of gels were obtained using Typhoon Trio Imager (Amersham Biosciences, Sweden).

2.8. ITC assays

ITC experiments to detect the binding of DNA to BioQ were performed at 25 °C using Auto-iTC200 titration calorimetry (MicroCal, United Kingdom). DNA (250 μM) was dissolved in 100 μl of reaction buffer containing 25 mM HEPES (pH 7.5) and 150 mM NaCl and titrated against 400 μl of 50 μM wild-type or mutant BioQ in the same buffer. The first injection (0.5 μl) was followed by 19 injections of 2 μl. The heat of dilution values for DNA was measured by injecting DNA into buffer alone. The values were subtracted from the experimental curves before data analysis. The stirring rate was 750 r.p.m. MicroCal ORIGIN software supplied with the instrument was used to determine the site-binding model that produced a good fit (low ×2 value) for the resulting data.

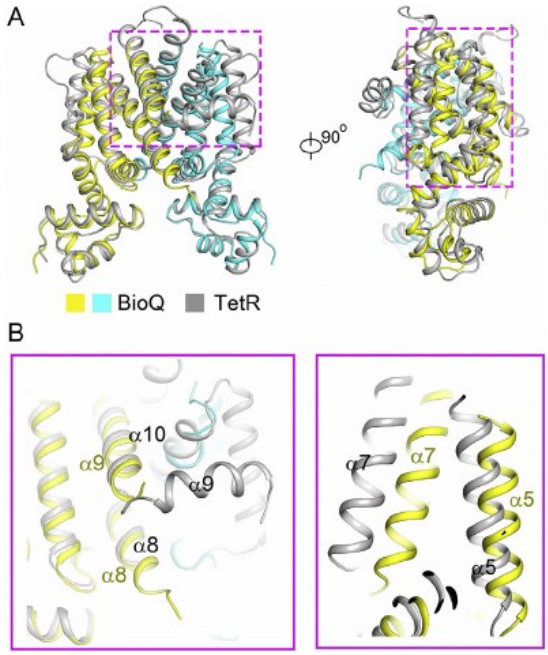

Fig. 3. Structural comparisons of BioQ with *E. coli* TetR. (A) Side views of the overall comparison of apo-BioQ and apo-TetR. The superposition is based on dimers. BioQ monomers are shown in cyan and yellow, respectively, while TetR (PBD: 1A6I) is shown in gray. (B) Enlarged views of the ligand-binding cavities colored as in (A).

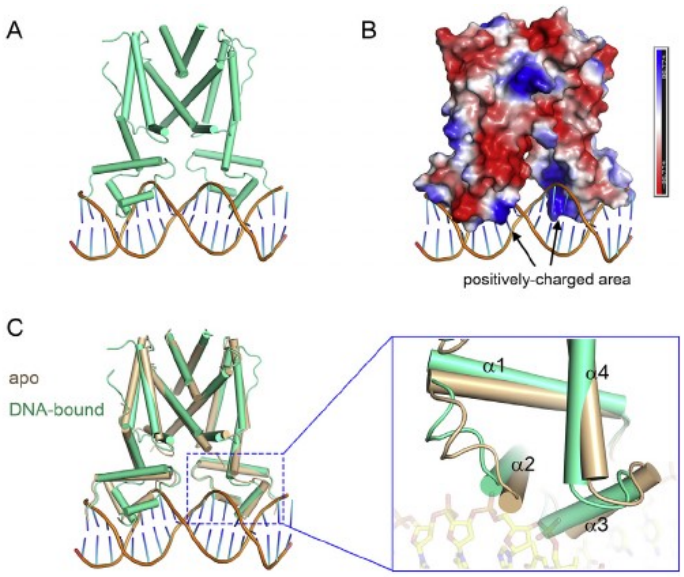

Fig. 4. Structure of the BioQ-operator complex. (A) Overall structure of the BioQ-operator complex. (B) Electrostatic surface potentials of BioQ. The blue regions indicate positive electrostatic regions, while red regions indicate negative electrostatic regions. (C) Structural comparison of apo-BioQ (wheat) with a DNA-bound BioQ (green cyan). The enlarged view of the DBD is shown in the right panel. Apo-BioQ and BioQ-operator exhibited an r.m.s. deviation of 1.8 Å over 288 Cα atoms.

2.9. Data access

Atomic coordinates and structure factors for the reported crystal structures have been deposited in the Protein Data Bank under the accession numbers 5YEK and 5YEJ.

3. Results

3.1. Overall structure of BioQ

We determined the apo-form crystal structure of BioQ (residues 1-188) at a resolution of 2.26 Å in space group I121 (Table 1). BioQ is a classical TFTR homodimer, with each protomer comprising 9 α helices: α1 (5-19), α2 (26-33), α3 (37-43), α4 (46-60), α5 (71-88), α6 (92-102), α7 (106-124), α8 (129-152), and α9 (170-188). There is no significant electron density for loop 64–68 or loop 155–169 connecting α8 and α9. Helices α1 to α3 form the DBD, and helices α4 to α9 form the LBD. The spacer helix α2 and recognition helix α3 constitute the HTH motif responsible for recognizing and binding DNA. Helix α4 links the DBD to the regulatory domain (Fig. 2).

We further compared BioQ to TetR, which is the first well-characterized TFTR member responsible for tetracycline resistance regulation [31–33]. BioQ shares a sequence identity of 28% with TetR. As shown in Fig. 3A, BioQ shares a high overall similarity with TetR with a root-mean-squared (r.m.s) deviation of 2.7 Å over 266 Cα atoms. Although both DBDs display similar folds, the LBD of BioQ exhibits two distinct features. The central part of the TetR LBD consists of anti-parallel helices α8 and α10, which play roles in ligand binding and dimerization [33]. The connecting helix, α9, plays a latch-like role in forming a ligand-binding pocket with three helices (α5, α7 and α8) of the other protomer. This essential helix is missing in BioQ and is instead replaced by a flexible loop (Fig. 3B). Furthermore, the angle between the α5 and α7 helices is much smaller than that of TetR. In line with the

Table 2
Operator sequences and helix 3–3′ distances of TFTRs.

Protein name	DNA operator (5′-3′)	Helix 3 - helix 3′(Å)		References
		Apo	DNA-bound	
BioQ	TGAACnnnGTTCA	38.9	35.3	
AibR	ACCTACCGnnCGGTAGGT	42.7	37.0	[34]
AmtR	CTATnnnnnnATAG	40.6	37.4	[37]
DesT	AGTGAACnnnnGTTGACT		38.6	[36]
HrtR	ATGACACnGTGTCAT	37.2	35.3	[38]
SimR	TTCGTACnnnGTACGAA	42.3	36.9	[35]
TetR	TCTATCAnTGATAGGA	38.8	34.7	[33]

structural observations, the DBD of BioQ shares high sequence similarity with other TFTRs, whereas the C-terminal regulatory domain exhibits broad sequence variation (Fig. S2), suggesting its diverse roles in multiple ligand recognition.

3.2. Structure of the BioQ-operator complex

To reveal the molecular basis of the operator recognition mechanism of BioQ, we determined the crystal structure of the BioQ homodimer in complex with its natural dsDNA operator (5′-ACCTGAACACCGTTCAAGT-3′), which is located in the promoter region of the *bioB* gene, at a resolution of 2.69 Å and refined it to an R_{work} of 21.3% and an R_{free} of 26.7% (Table 1). In the DNA-bound complex, each DBD directly binds to the conserved operator sequence (5′-CCTGAACA-3′ and 5′-CGTTCAAG-3′), where helices α2 (α2′) and α3 (α3′) insert into the major groove (Fig. 4A). Furthermore, the DBD is rich in positively charged residues at the DNA operator interface, which interacts with the phosphate group to stabilize the complex (Fig. 4B).

The BioQ homodimer undergoes a conformational change upon binding to DNA. In the BioQ-operator complex, helices α2, α3 and α4 of one monomer are pulled towards the other, moderately decreasing the separation between the recognition helices α3 and α3′ (Fig. 4C and Table 2). The interhelical distance between helix α3 and α3′ is 38.9 Å, while that of DNA-bound BioQ is narrowed to 35.3 Å. Consistent with this observation, other TFTR family members also undergo a similar helix α3–3′ distance reduction upon DNA binding (Table 2) [33–38], suggesting a conserved DNA regulation role for TFTRs.

The conformational parameters of both canonical DNA and BioQ-bound DNA were calculated using a previously reported method [39] to characterize the conformational change in the BioQ-operator upon binding to BioQ. In the complex, the operator displays average global roll and twist angles of 3.6 Å and 32.8 Å, respectively, indicating that the overall conformation of the 19-bp DNA is that of a typical B-form DNA (compared with the roll and twist values of 0 Å and 36.0 Å, respectively, for an idealized B-form DNA) (Figs. 5A and B). The major groove on the opposite side of the BioQ interface remains unchanged, but the major groove at the recognition site is widened to 12.9–14.2 Å, which is higher than the typical distance of 11.4 Å in canonical B-form DNA (Fig. 5C). Furthermore, the average minor groove width is 7.6 Å, which represents a significant increase (canonical B-form DNA width is 5.9 Å) (Fig. 5D). Taken together, these findings show that the insertion of helix α3 of BioQ into the major groove at the recognition site results in operator deformation.

3.3. DNA recognition by BioQ

The BioQ-operator complex structure shows that the 19-mer dsDNA operator is bound by a BioQ homodimer, and the half-site of the palindromic operator is symmetrically recognized by two DBDs from each protomer. Each half of the operator is stabilized by a total of 9 phosphate backbones and 1 direct base contacts, as shown in Fig. 6A. Thr25 and Arg27 from helix α2; Thr36, Tyr41, Trp42 and His43 from helix α3; and Lys47 from helix α4 penetrate the major groove of operator DNA and make direct contact with the DNA.

The phosphate backbones of the 5′-terminal half of the BioQ-operator (5′-ACCTGAACA-3′) are coordinated by six charged or polar amino acids. Trp42, His43 and Thr36 contact the phosphates from the sense strand via C2, C3 and T4 (Fig. 6A and B, Fig. S3A), while Thr25, Lys47 and Tyr41 interact with them from the antisense strand via T11′, G12′ and T13′, respectively (Fig. 6A and C, Fig. S3B). We speculate that these residues determine the length of the BioQ operator. Supporting these salt-bridge interactions, Arg27 coordinates with the guanine at position 12 via hydrogen bonds, contributing to the DNA-binding affinity (Figs. 6A and C, Fig. S3B). To investigate whether other base pairs participate in BioQ interaction, we mutated all DNA sequences individually and measured the binding affinity of BioQ with the 19-bp mutated DNA sequences (Table S2). Mutations in other unrelated bases had little effect on DNA binding, but mutation of C8 (G12') to purine resulted in several orders of reduction or complete loss of DNA affinity, consistent with structural observations.

3.4. Critical amino acid residues responsible for the BioQ-operator interaction

The importance of amino acid residues in DNA recognition is

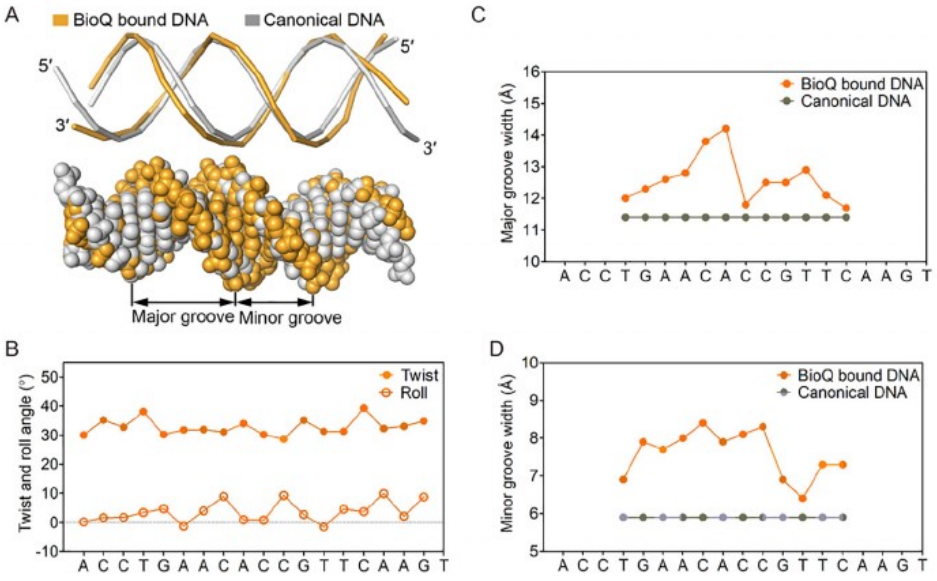

Fig. 5. DNA deformation in the BioQ-DNA complex. (A) Structural comparison of the double helix of BioQ-bound DNA with canonical B-form DNA. BioQ-bound DNA is highlighted in yellow, while canonical B-form DNA is shown in gray. (B) The roll and twist angles for each base pair step of the BioQ-bound DNA. (C) The major groove width of the BioQ-bound DNA and canonical B-form DNA. (D) The minor groove width of the BioQ-bound DNA and canonical B-form DNA.

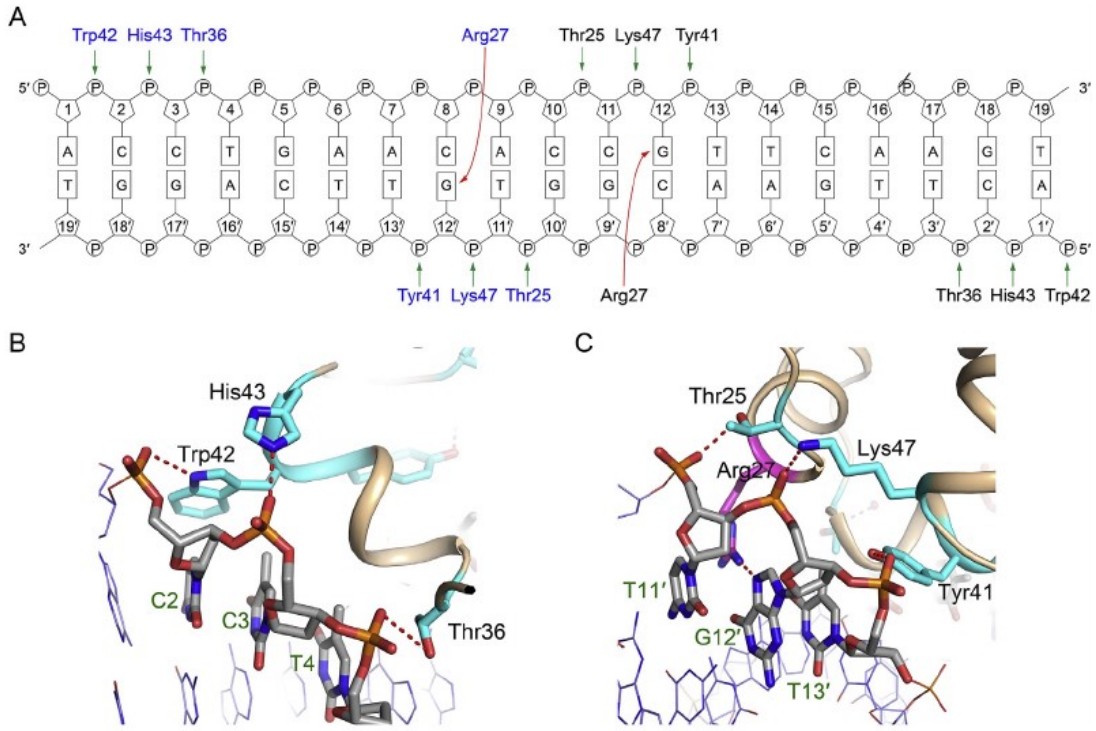

Fig. 6. Interactions of BioQ with the operator DNA. (A) Schematic representation of BioQ-operator interactions. Red arrows indicate a base-specific hydrogen bond, and green arrows indicate the phosphate backbone contacts. The sense and antisense strand sequences of the BioQ operator are shown with the bases numbered from 1 to 19, and 1′ to 19′, respectively. Amino acid residues from two protomers are indicated by blue and black. The schematic was generated using NuProPlot (http://www.nuproplot.com/). (B) and (C) Close-up view of the BioQ-DNA interface within the protomer. Amino acid residue interacting with the base (G12′) is colored in pink, while the residues that interact with phosphate backbones are colored in blue. DNA phosphate backbones and bases are colored in orange and gray, respectively.

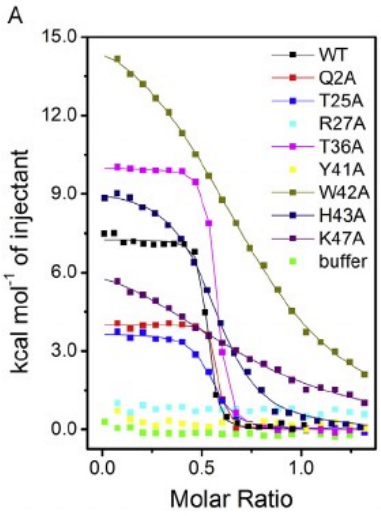

Protein	K_d (nM)
Wild Type	13.8 ± 5.7
Q2A	18.0 ± 8.9
T25A	265.2 ± 56.0
R27A	*NB
T36A	53.8 ± 3.0
Y41A	*NB
W42A	6097.6 ± 196.7
H43A	1190.4 ± 87.0
K47A	11325.0 ± 1176.1

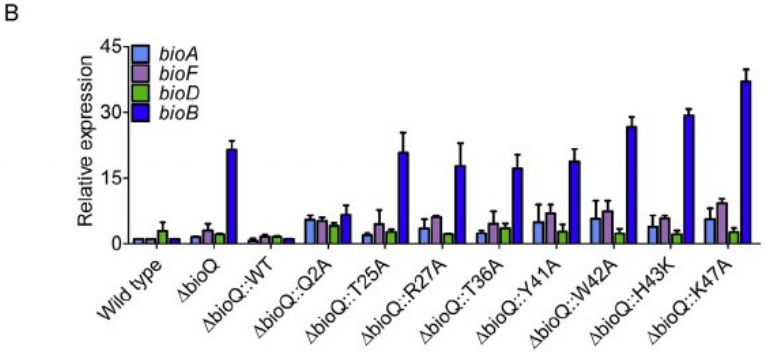

Fig. 7. Identification of critical residues for DNA binding by site-directed mutagenesis. (A) ITC assay of BioQ variants with the wild-type operator. The isothermal titration curves of the interactions between BioQ variants and the wild-type operator are shown. The calculated K_d values are indicated. *NB represents no detectable binding activity by ITC. (B) Characterization of the regulatory role of BioQ and its mutants in vivo. Relative expression of the *bioA*, *bioF*, *bioD* and *bioB* genes was quantified using qRT-PCR in wild-type *M. smegmatis*, Δ*bioQ*, and its complementary strains, which expressed BioQ and the mutant proteins as indicated in (A). The qRT-PCR data were collected from two independent biological replicates and expressed as the means ± standard deviation (SD).

supported by mutational analysis. The residues Thr25, Arg27, Thr36, Tyr41, Trp42, His43 and Lys47, as well as the control residue Gln2, which does not directly interact with DNA, were substituted by alanine. The DNA-binding abilities of the mutants were measured via ITC. As shown in Fig. 7A, wild-type BioQ showed apparent DNA-binding ability with a dissociated constant (K_d) value of approximately 13.8 nM and also bound the nonsense mutant (Q2A). Several alanine substitutions, such as T25A, W42A, H43A, and K47A, resulted in dramatic decreases in DNA-binding ability, while the T36A mutation slightly affected DNA-binding. Specially, R27A and Y41A completely abolished DNA targeting. The loss of DNA binding was not due to structural disruption, because the mutants exhibited the same solution behavior as wide-type BioQ via gel filtration (Fig. S4).

This result was corroborated by transcription analysis in vivo. BioQ is a transcriptional repressor in *M. smegmatis* and represses the transcription of the *bioF*, *bioD* and *bioB* genes; among these genes, the expression of the *bioB* gene is strongly repressed because its promoter possesses two BioQ binding sites [14]. The expression of *bioB* was significantly higher in the BioQ-deficient mutant Δ*bioQ* than in wild-type *M. smegmatis*. The complementary strain Δ*bioQ*::WT, which expresses wild-type BioQ, restored *bioB* expression levels to those of the wild-type strain. Expression of BioQ mutants (T25A, R27A, T36A, Y41A, W42A, H43A and K47A) with decreased DNA-binding ability in Δ*bioQ* did not repress the expression of *bioB*, whereas Q2A fully compensated for the suppressive function of BioQ by restoring expression to wild-type levels (Fig. 7B). Additionally, most of these residues are highly conserved in TFTR members (Fig. S2). Taken together, these findings characterized the essential residues involved in DNA binding in the TFTR family.

4. Discussion

Mycobacterium strains lack a biotin uptake system. Therefore, their primary source of biotin is from de novo synthesis [40,41]. Biotin synthesis deficiency in *M. tuberculosis* has been found to cause severe growth defects with decreasing virulence [42]. Thus, the bacterial biotin synthetic pathway is a potential anti-tuberculosis drug target [41,43]. BioQ is a new transcriptional repressor for biotin synthesis in *Mycobacterium*. However, the structural basis for the transcriptional regulation of BioQ remains unknown. Here, we determined the crystal structures of BioQ and the BioQ-operator complex and elucidated the DNA recognition mechanism. Although BioQ shares sequence and structural similarity with other typical TFTR family members, it exhibits several distinct structural features for DNA recognition. First, helix α2 contains Arg27 and Thr25, which are involved in direct interactions with the DNA base and phosphate backbone, respectively, indicating that α2 functions as a primary helix for DNA-binding activity, unlike the observation that helix α3 is usually responsible for DNA recognition in typical TFTRs [33,35]. However, the whole α3 helix of BioQ was found to insert into the major groove and directly contact the DNA phosphate backbone via residues Thr36, Tyr41, Trp42 and His43, strengthening BioQ-DNA binding activity. Interestingly, the α4 helix was previously found to serve as a connector helix that transmits information between TFTRs in various states [35,44,45]. However, we found that the ε-amino moiety of Lys47 from the α4 helix of BioQ also forms a hydrogen bond with the phosphate backbone. As shown in Fig. 7, most alanine substitutions, such as T25A, R27A, Y41A, W42A, H43A and K47A, resulted in significant reduction in DNA-binding affinities, while T36A retained one quarter of the DNA-binding ability compared with that of wild-type BioQ. These residues seem to contribute to the DNA binding in different ways, with their binding affinities exhibiting a wide range of K_d values. Interestingly, when these mutations were expressed in complementary strains, *bioB* expression levels were higher than those of the wild type, indicating that all residues are required for the proper transcriptional function. Taken together, these results suggest that there is a DNA-binding affinity threshold for the in vivo function of BioQ.

Previous studies identified a 13 bp sequence (5′-TGAACnnnGTTCA-3′) containing two perfect reverse complementary sequences separated by three nucleotides, as the BioQ binding site [14,15]. Based on the complex structure of BioQ with the 19-bp operator (5′-ACCTGAACAC CGTTCAAGT-3′), the phosphate backbones of C2, C3 and T4 were found to directly interact with Trp42, His43 and Thr36 of BioQ, respectively (Fig. 6A). We also investigated whether other sequences in the operator engage in BioQ binding via ITC (Table S2 and Fig. S5). As shown Fig. S5, a palindromic sequence (5′-TGAACnnnGTTCA-3′) is crucial for BioQ binding, and mutation of any bases in this region resulted in significant changes in binding affinity. Based on the structure of BioQ in complex with DNA, there is only one base-specific interaction: between Arg27 and base C8/G12′. C8G mutation completely abolished binding, and C8A mutation led to a ~4000-fold decrease in affinity (Table S2). BioQ also employs a motif comprising six amino acids for DNA backbone interactions. For example, Tyr41 interacts with the phosphate group of T13′, and mutation of this residue completely abolished DNA targeting. Similarly, A7/T13′ mutations resulted in large changes in affinity by 100-300-fold. T4G also notably affects in the binding affinity, possibly by altering the binding of BioQ to the phosphate group. Mutations in position G5 resulted in a 10-fold reduction in affinity with the exception of G5A, in which one purine was replaced by the other type of purine. In contrast, the bases in the space or wings of the two palindromic sequences play negligible roles in protein binding. Mutations in these regions showed little change in binding affinity (Fig. S5).

TFTRs are known for their ability to bind with diverse ligands. Canonical TFTRs, such as TetR, FadR and HrtR, are targeted to the promoter region to repress gene transcription, and specific ligand binding in the LBD domain usually abolishes the DNA binding activity to release the repression effect as a consequence [38,46–50]. However, some multidrug binding proteins, including RamR, QacR and CgmR, are able to respond to various ligands [22–24]. In some cases, noncanonical TFTRs, such as DesT, also bind to two different ligands, and DNA-binding ability is stimulated by binding unsaturated acyl-CoA at the allosteric sites but is inhibited by binding saturated acyl-CoA [36]. Furthermore, AibR, another noncanonical TFTR, does not block transcription in the ligand-free state but blocks transcription in the ligand-bound state [34]. For decades, a plethora of TFTR members have been identified with their target sequences. However, limited information about their ligands impedes the functional study of gene regulation [45,51–61].

We have determined the structure of BioQ alone and in complex with its operator but have thus far failed to identify its ligand. However, structural analysis of BioQ as well as other TFTR members may provide a possible explanation (Fig. S6A and B). Based on the ligand-bound structures of TFTRs, the small ligand molecules are locked into the ligand-binding pocket, which is composed of helices α5, α7, and α8 from one protomer, and an additional helix from the other protomer acting as a latch. The latch sterically blocks the cavity and directly interacts with the ligand to stabilize the conformation of the TetR-ligand complex. In BioQ, the latch-like helix is replaced by a short, flexible loop (Fig. 3B). Furthermore, we found that other TFTR members, including AefR [62] and HapR [63] whose ligands are unknown, also possess short latches, resulting in open ligand binding cavities (Fig. S6A). TFTR members whose ligands have been identified, such as TetR [31], AibR [34] and SimR [64], have large latches composed of helices and loops (Fig. S6B). Thus, we hypothesize that the latch of BioQ is too short to cover the binding cavity, which may lead to a more flexible conformation of the BioQ-ligand complex, making it difficult to identify the ligand. Nevertheless, the possibility that the flexible loop may be structured in the presence of ligand should not be excluded. Further studies are needed to identify the physiological ligand of BioQ.

Acknowledgments

This work was supported by the National Natural Science Foundation of China [grant numbers 81601742, 31770087], the Fundamental Research Funds for the Central Universities [grant numbers 2662014BQ028, 2662017PY112] and the China Postdoctoral Science Foundation [grant number 2017M622472].

We greatly appreciate Dr. Youjun Feng of Zhejiang University for expertise and assistance in experimental design. We would like to acknowledge Jianhua He at the Shanghai Synchrotron Radiation Facility (SSRF) beamline 216 BL17U and Rongguang Zhang at the SSRF beamline BL19U for on-site assistance. We thank research associates at the Center for Protein Research, Huazhong Agricultural University, for technical support. We also thank Zhao Yang for contributing to the site-directed mutagenesis experiments and protein crystallization.

Appendix A. Supplementary data

Supplementary data to this article can be found online at https://doi.org/10.1016/j.bbagen.2018.05.015.

References

[1] J.E. Cronan, Biotin and Lipoic Acid: Synthesis, Attachment, and Regulation, EcoSal Plus 6 (2014) 1–37 https://doi.org/10.1128/ecosalplus.ESP-0001-2012.
[2] D. Beckett, Biotin sensing: universal influence of biotin status on transcription, Annu. Rev. Genet. 41 (2007) 443–464 https://doi.org/10.1146/annurev.genet.41.042007.170450.
[3] W.R. Streit, P. Entcheva, Biotin in microbes, the genes involved in its biosynthesis, its biochemical role and perspectives for biotechnological production, Appl. Microbiol. Biotechnol. 61 (2003) 21–31 https://doi.org/10.1007/s00253-002-1186-2.
[4] D. Pacheco-Alvarez, R.S. Solorzano-Vargas, A.L. Del Rio, Biotin in metabolism and its relationship to human disease, Arch. Med. Res. 33 (2002) 439–447 https://www.ncbi.nlm.nih.gov/pubmed/12459313.
[5] Y. Feng, H. Zhang, J.E. Cronan, Profligate biotin synthesis in alpha-proteobacteria - a developing or degenerating regulatory system? Mol. Microbiol. 88 (2013) 77–92 https://doi.org/10.1111/mmi.12170.
[6] K. Balamurugan, A. Ortiz, H.M. Said, Biotin uptake by human intestinal and liver epithelial cells: role of the SMVT system, Am. J. Physiol. Gastrointest. Liver Physiol. 285 (2003) G73–G77 https://doi.org/10.1152/ajpgi.00059.2003.
[7] H.M. Said, Cell and molecular aspects of human intestinal biotin absorption, J. Nutr. 139 (2009) 158–162 https://doi.org/10.3945/jn.108.092023.
[8] D.A. Rodionov, M.S. Gelfand, Computational identification of BioR, a transcriptional regulator of biotin metabolism in Alphaproteobacteria, and of its binding signal, FEMS Microbiol. Lett. 255 (2006) 102–107 https://doi.org/10.1111/j.1574-6968.2005.00070.x.
[9] S. Lin, J.E. Cronan, Closing in on complete pathways of biotin biosynthesis, Mol. BioSyst. 7 (2011) 1811–1821 https://doi.org/10.1039/c1mb05022b.
[10] G. Schneider, Y. Lindqvist, Structural enzymology of biotin biosynthesis, FEBS Lett. 495 (2001) 7–11.
[11] S.H. Fan, D.F. Li, D.C. Wang, J. Fleming, H.T. Zhang, Y. Zhou, et al., Structure and function of *Mycobacterium smegmatis* 7-keto-8-aminopelargonic acid (KAPA) synthase, Int. J. Biochem. Cell Biol. 58 (2015) 71–80 https://doi.org/10.1016/j.biocel.2014.11.006.
[12] S. Fan, D. Li, J. Fleming, Y. Hong, T. Chen, L. Zhou, et al., Purification and X-ray crystallographic analysis of 7-keto-8-aminopelargonic acid (KAPA) synthase from *Mycobacterium smegmatis*, Acta Crystallogr. F Struct. Biol. Commun. 70 (2014) 1372–1375 https://doi.org/10.1107/S2053230X14018317.
[13] D.A. Rodionov, A.A. Mironov, M.S. Gelfand, Conservation of the biotin regulon and the BirA regulatory signal in eubacteria and archaea, Genome Res. 12 (2002) 1507–1516 https://doi.org/10.1101/gr.314502.
[14] Q. Tang, X. Li, T. Zou, H. Zhang, Y. Wang, R. Gao, et al., *Mycobacterium smegmatis* BioQ defines a new regulatory network for biotin metabolism, Mol. Microbiol. 94 (2014) 1006–1023 https://doi.org/10.1111/mmi.12817.
[15] I. Brune, S. Gotker, J. Schneider, D.A. Rodionov, A. Tauch, Negative transcriptional control of biotin metabolism genes by the TetR-type regulator BioQ in biotin-auxotrophic *Corynebacterium glutamicum* ATCC 13032, J. Biotechnol. 159 (2012) 225–234 https://doi.org/10.1016/j.jbiotec.2011.12.001.
[16] M.D. Routh, C.C. Su, Q. Zhang, E.W. Yu, Structures of AcrR and CmeR: insight into the mechanisms of transcriptional repression and multi-drug recognition in the TetR family of regulators, Biochim. Biophys. Acta 1794 (2009) 844–851 https://doi.org/10.1016/j.bbapap.2008.12.001.
[17] W. Deng, C. Li, J. Xie, The underling mechanism of bacterial TetR/AcrR family transcriptional repressors, Cell. Signal. 25 (2013) 1608–1613 https://doi.org/10.1016/j.cellsig.2013.04.003.
[18] J.L. Ramos, M. Martinez-Bueno, A.J. Molina-Henares, W. Teran, K. Watanabe, X. Zhang, et al., The TetR family of transcriptional repressors, Microbiol. Mol. Biol. Rev. 69 (2005) 326–356 https://doi.org/10.1128/MMBR.69.2.326-356.2005.
[19] L. Cuthbertson, J.R. Nodwell, The TetR family of regulators, Microbiol. Mol. Biol. Rev. 77 (2013) 440–475 https://doi.org/10.1128/MMBR.00018-13.
[20] R.J. Balhana, A. Singla, M.H. Sikder, M. Withers, S.L. Kendall, Global analyses of TetR family transcriptional regulators in mycobacteria indicates conservation across species and diversity in regulated functions, BMC Genomics 16 (2015) 479 https://doi.org/10.1186/s12864-015-1696-9.
[21] Z. Yu, S.E. Reichheld, A. Savchenko, J. Parkinson, A.R. Davidson, A comprehensive analysis of structural and sequence conservation in the TetR family transcriptional regulators, J. Mol. Biol. 400 (2010) 847–864 https://doi.org/10.1016/j.jmb.2010.05.062.
[22] S. Yamasaki, E. Nikaido, R. Nakashima, K. Sakurai, D. Fujiwara, I. Fujii, et al., The crystal structure of multidrug-resistance regulator RamR with multiple drugs, Nat. Commun. 4 (2013) 2078 https://doi.org/10.1038/ncomms3078.
[23] M.A. Schumacher, M.C. Miller, S. Grkovic, M.H. Brown, R.A. Skurray, R.G. Brennan, Structural mechanisms of QacR induction and multidrug recognition, Science 294 (2001) 2158–2163 https://doi.org/10.1126/science.1066020.
[24] H. Itou, N. Watanabe, M. Yao, Y. Shirakihara, I. Tanaka, Crystal structures of the multidrug binding repressor *Corynebacterium glutamicum* CgmR in complex with inducers and with an operator, J. Mol. Biol. 403 (2010) 174–184 https://doi.org/10.1016/j.jmb.2010.07.042.
[25] Q.S. Wang, F. Yu, S. Huang, B. Sun, K.H. Zhang, K. Liu, et al., The macromolecular crystallography beamline of SSRF, Nucl. Sci. Tech. 26 (2015) 12–17 https://www.researchgate.net/publication/292831461.
[26] Z. Otwinowski, W. Minor, Processing of X-ray diffraction data collected in oscillation mode, Methods Enzymol. 276 (1997) 307–326 https://www.ncbi.nlm.nih.gov/pubmed/27754618.
[27] M.D. Winn, C.C. Ballard, K.D. Cowtan, E.J. Dodson, P. Emsley, P.R. Evans, et al., Overview of the CCP4 suite and current developments, Acta Crystallogr. D Biol. Crystallogr. 67 (2011) 235–242 https://doi.org/10.1107/S0907444910045749.
[28] A.J. McCoy, R.W. Grosse-Kunstleve, P.D. Adams, M.D. Winn, L.C. Storoni, R.J. Read, Phaser crystallographic software, J. Appl. Crystallogr. 40 (2007) 658–674 https://doi.org/10.1107/S0021889807021206.
[29] K. Cowtan, P. Emsley, Coot: model-building tools for molecular graphics, Acta Crystallogr. D Biol. Crystallogr. 60 (2004) 2126–2132 https://doi.org/10.1107/S0907444904019158.
[30] P.D. Adams, R.W. Grosse-Kunstleve, L.W. Hung, T.R. Ioerger, A.J. McCoy, N.W. Moriarty, et al., PHENIX: building new software for automated crystallographic structure determination, Acta Crystallogr. D Biol. Crystallogr. 58 (2002) 1948–1954 https://www.ncbi.nlm.nih.gov/pubmed/12393927.
[31] W. Hinrichs, C. Kisker, M. Duvel, A. Muller, K. Tovar, W. Hillen, et al., Structure of the Tet repressor-tetracycline complex and regulation of antibiotic resistance, Science 264 (1994) 418–420 http://science.sciencemag.org/content/264/5157/418.
[32] C. Kisker, W. Hinrichs, K. Tovar, W. Hillen, W. Saenger, The complex formed between Tet repressor and tetracycline-Mg^{2+} reveals mechanism of antibiotic resistance, J. Mol. Biol. 247 (1995) 260–280 https://www.ncbi.nlm.nih.gov/pubmed/7707374.
[33] P. Orth, D. Schnappinger, W. Hillen, W. Saenger, W. Hinrichs, Structural basis of gene regulation by the tetracycline inducible Tet repressor-operator system, Nat. Struct. Biol. 7 (2000) 215–219 https://doi.org/10.1038/73324.
[34] T. Bock, C. Volz, V. Hering, A. Scrima, R. Muller, W. Blankenfeldt, The AibR-isovaleryl coenzyme A regulator and its DNA binding site - a model for the regulation of alternative de novo isovaleryl coenzyme A biosynthesis in *Myxococcus xanthus*, Nucleic Acids Res. 45 (2017) 2166–2178 https://doi.org/10.1093/nar/gkw1238.
[35] T.B. Le, M.A. Schumacher, D.M. Lawson, R.G. Brennan, M.J. Buttner, The crystal structure of the TetR family transcriptional repressor SimR bound to DNA and the role of a flexible N-terminal extension in minor groove binding, Nucleic Acids Res. 39 (2011) 9433–9447 https://doi.org/10.1093/nar/gkr640.
[36] D.J. Miller, Y.M. Zhang, C. Subramanian, C.O. Rock, S.W. White, Structural basis for the transcriptional regulation of membrane lipid homeostasis, Nat. Struct. Mol. Biol. 17 (2010) 971–975 https://doi.org/10.1038/nsmb.1847.
[37] C. Palanca, V. Rubio, Structure of AmtR, the global nitrogen regulator of *Corynebacterium glutamicum*, in free and DNA-bound forms, FEBS J. 283 (2016) 1039–1059 https://doi.org/10.1111/febs.13643.
[38] H. Sawai, M. Yamanaka, H. Sugimoto, Y. Shiro, S. Aono, Structural basis for the transcriptional regulation of heme homeostasis in *Lactococcus lactis*, J. Biol. Chem. 287 (2012) 30755–30768 https://doi.org/10.1074/jbc.M112.370916.
[39] G. Zheng, X.J. Lu, W.K. Olson, Web 3DNA - a web server for the analysis, reconstruction, and visualization of three-dimensional nucleic-acid structures, Nucleic Acids Res. 37 (2009) W240–W246 https://doi.org/10.1093/nar/gkp358.
[40] W. Salaemae, A. Azhar, G.W. Booker, S.W. Polyak, Biotin biosynthesis in *Mycobacterium tuberculosis*: physiology, biochemistry and molecular intervention, Protein Cell 2 (2011) 691–695 https://doi.org/10.1007/s13238-011-1100-8.
[41] S.W. Park, D.E. Casalena, D.J. Wilson, R. Dai, P.P. Nag, F. Liu, et al., Target-based identification of whole-cell active inhibitors of biotin biosynthesis in *Mycobacterium tuberculosis*, Chem. Biol. 22 (2015) 76–86 https://doi.org/10.1016/j.chembiol.2014.11.012.
[42] P.Nangpal Nangpal, R. Kar, S. Mathur, A.K. Tyagi, bioA mutant of *Mycobacterium tuberculosis* shows severe growth defect and imparts protection against tuberculosis in guinea pigs, PLoS One 12 (2017), https://doi.org/10.1371/journal.pone.0179513.
[43] S. Mann, S. Carillon, O. Breyne, A. Marquet, Total synthesis of amiclenomycin, an inhibitor of biotin biosynthesis, Chemistry 8 (2002) 2–5, http://dx.doi.org/10.1002/1521-3765(20020118)8:2<439::AID-CHEM439>3.0.CO.
[44] H. Bhukya, R. Bhujbalrao, A. Bitra, R. Anand, Structural and functional basis of transcriptional regulation by TetR family protein CprB from *S. coelicolor A3(2)*,

Nucleic Acids Res. 42 (2014) 10122–10133 https://doi.org/10.1093/nar/gku587.
[45] S.F. Yang, Z.Q. Gao, T.T. Li, M. Yang, T.Y. Zhang, Y.H. Dong, et al., Structural basis for interaction between *Mycobacterium smegmatis* Ms6564, a TetR family master regulator, and its target DNA, J. Biol. Chem. 288 (2013) 23687–23695 https://doi.org/10.1074/jbc.M113.468694.
[46] Y. Agari, K. Agari, K. Sakamoto, S. Kuramitsu, A. Shinkai, TetR-family transcriptional repressor *Thermus thermophilus* FadR controls fatty acid degradation, Microbiology 157 (2011) 1589–1601 https://doi.org/10.1099/mic.0.048017-0.
[47] N.A. Ho, S.S. Dawes, A.M. Crowe, I. Casabon, C. Gao, S.L. Kendall, et al., The structure of the transcriptional repressor KstR in complex with CoA thioester cholesterol metabolites sheds light on the regulation of cholesterol catabolism in *Mycobacterium tuberculosis*, J. Biol. Chem. 291 (2016) 7256–7266 https://doi.org/10.1074/jbc.M115.707760.
[48] J.R. Bolla, S.V. Do, F. Long, L. Dai, C.C. Su, H.T. Lei, et al., Structural and functional analysis of the transcriptional regulator Rv3066 of *Mycobacterium tuberculosis*, Nucleic Acids Res. 40 (2012) 9340–9355 https://doi.org/10.1093/nar/gks677.
[49] H.K. Yeo, Y.W. Park, J.Y. Lee, Structural basis of operator sites recognition and effector binding in the TetR family transcription regulator FadR, Nucleic Acids Res. 45 (2017) 4244–4254 https://doi.org/10.1093/nar/gkx009.
[50] J.A. Delmar, T.H. Chou, C.C. Wright, M.H. Licon, J.K. Doh, A. Radhakrishnan, et al., Structural basis for the regulation of the MmpL transporters of *Mycobacterium tuberculosis*, J. Biol. Chem. 290 (2015) 28559–28574 https://doi.org/10.1074/jbc.M115.683797.
[51] H. Bhukya, A.K. Jana, N. Sengupta, R. Anand, Structural and dynamics studies of the TetR family protein, CprB from *Streptomyces coelicolor* in complex with its biological operator sequence, J. Struct. Biol. 198 (2017) 134–146 https://doi.org/10.1016/j.jsb.2017.03.006.
[52] Y. Alguel, D. Lu, N. Quade, S. Sauter, X. Zhang, Crystal structure of MexZ, a key repressor responsible for antibiotic resistance in *Pseudomonas aeruginosa*, J. Struct. Biol. 172 (2010) 305–310 https://doi.org/10.1016/j.jsb.2010.07.012.
[53] W. Chen, D. Wang, W. Zhou, H. Sang, X. Liu, Z. Ge, et al., Novobiocin binding to NalD induces the expression of the MexAB-OprM pump in *Pseudomonas aeruginosa*, Mol. Microbiol. 100 (2016) 749–758 https://doi.org/10.1111/mmi.13346.
[54] Y. Agari, K. Sakamoto, K. Yutani, S. Kuramitsu, A. Shinkai, Structure and function of a TetR family transcriptional regulator, SbtR, from *Thermus thermophilus* HB8, Proteins 81 (2013) 1166–1178 https://doi.org/10.1002/prot.24266.
[55] D. Xu, P. Waack, Q. Zhang, S. Werten, W. Hinrichs, M.J. Virolle, Structure and regulatory targets of SCO3201, a highly promiscuous TetR-like regulator of *Streptomyces coelicolor* M145, Biochem. Biophys. Res. Commun. 450 (2014) 513–518 https://doi.org/10.1016/j.bbrc.2014.06.003.
[56] Y. Kim, B.S. Kim, Y.J. Park, W.C. Choi, J. Hwang, B.S. Kang, et al., Crystal structure of SmcR, a quorum-sensing master regulator of *Vibrio vulnificus*, provides insight into its regulation of transcription, J. Biol. Chem. 285 (2010) 14020–14030 https://doi.org/10.1074/jbc.M109.100248.
[57] H. Sugino, T. Usui, T. Shimada, M. Nakano, H. Ogasawara, A. Ishihama, et al., A structural sketch of RcdA, a transcription factor controlling the master regulator of biofilm formation, FEBS Lett. 591 (2017) 2019–2031 https://doi.org/10.1002/1873-3468.12713.
[58] Y. Kim, Y. Kang, J. Choe, Crystal structure of *Pseudomonas aeruginosa* transcriptional regulator PA2196 bound to its operator DNA, Biochem. Biophys. Res. Commun. 440 (2013) 317–321 https://doi.org/10.1016/j.bbrc.2013.09.074.
[59] S.H. Kim, H.N. Lee, H.J. Kim, E.S. Kim, Transcriptome analysis of an antibiotic downregulator mutant and synergistic Actinorhodin stimulation via disruption of a precursor flux regulator in *Streptomyces coelicolor*, Appl. Environ. Microbiol. 77 (2011) 1872–1877 https://doi.org/10.1128/AEM.02346-10.
[60] S. Ray, A. Maitra, A. Biswas, S. Panjikar, J. Mondal, R. Anand, Functional insights into the mode of DNA and ligand binding of the TetR family regulator TylP from *Streptomyces fradiae*, J. Biol. Chem. 292 (2017) 15301–15311 https://doi.org/10.1074/jbc.M117.788000.
[61] T. Hayashi, Y. Tanaka, N. Sakai, U. Okada, M. Yao, N. Watanabe, et al., Structural and genomic DNA analysis of the putative TetR transcriptional repressor SCO7518 from *Streptomyces coelicolor* A3(2), FEBS Lett. 588 (2014) 4311–4318 https://doi.org/10.1016/j.febslet.2014.09.037.
[62] B. Quinones, C.J. Pujol, S.E. Lindow, Regulation of AHL production and its contribution to epiphytic fitness in *Pseudomonas syringae*, Mol. Plant-Microbe Interact. 17 (2004) 521–531 https://doi.org/10.1094/MPMI.2004.17.5.521.
[63] R.S. De Silva, G. Kovacikova, W. Lin, R.K. Taylor, K. Skorupski, F.J. Kull, Crystal structure of the *Vibrio cholerae* quorum-sensing regulatory protein HapR, J. Bacteriol. 189 (2007) 5683–5691 https://doi.org/10.1128/JB.01807-06.
[64] T.B.K. Le, C.E.M. Stevenson, H.P. Fiedler, A. Maxwell, D.M. Lawson, M.J. Buttner, Structures of the TetR-like simocyclinone efflux pump repressor, SimR, and the mechanism of ligand-mediated derepression, J. Mol. Biol. 408 (2011) 40–56 https://doi.org/10.1016/j.jmb.2011.02.035.
[65] P.A. Karplus, K. Diederichs, Linking crystallographic model and data quality, Science 336 (2012) 1030–1033 https://doi.org/10.1126/science.1218231.
[66] I.W. Davis, L.W. Murray, J.S. Richardson, D.C. Richardson, MolProbity: structure validation and all-atom contact analysis for nucleic acids and their complexes, Nucleic Acids Res. 32 (2004) W615–W619 https://doi.org/10.1093/nar/gkh398.